Journal of Structural Geology 31 (2009) 637–653

Contents lists available at ScienceDirect

Journal of Structural Geology

journal homepage: www.elsevier.com/locate/jsg

Quantifying granular material and deformation: Advantages of combining grain size, shape, and mineral phase recognition analysis

T.E. Bjørk*, K. Mair, H. Austrheim

Physics of Geological Processes (PGP), University of Oslo, PO Box 1048, Blindern, 0316 Oslo, Norway

ARTICLE INFO

Article history:
Received 24 January 2008
Received in revised form
10 February 2009
Accepted 2 March 2009
Available online 15 April 2009

Keywords:
Fault rocks
Particle size distribution
Grain shape
Digital image analysis

ABSTRACT

Granular material from a fault and a clastic dike in granodiorite at the NW contact of the Hornelen basin has been compared by a new digital image analysis tool to extract size and shape characteristics for individual phases.

Particle size distributions measured in both samples are consistent with shear fracturing ($D \sim 3.0$–3.2). However, the shape characteristics of the samples are distinct. Granular material from the dike shows no clear shape–size relationship. In contrast, granular material from the fault shows a systematic shape–size relationship (smaller grains being circular and smoother) suggesting a shift in deformation mechanism from intragranular fracturing to abrasion with decreasing grain size. Similarly, field observations, petrography, and the shape and texture of epidote indicate repeated faulting events. Field and textural observations combined with grain size and shape characteristics indicate that the dike sample has a mixed origin. Granulation in fractures connecting to the dike indicates mechanical deformation, while flow structures, texture, grain shape, and high content of epidote in the dike itself suggest that basinal fluids were present.

We show that combined size, shape and phase recognition analyses can reveal quantifiable differences in the granular material associated with a fault and a clastic dike, hence allowing us to interpret the distinct origin of these materials.

1. Introduction

Deformation of fault rock material is characterized by the development of a structural fabric or texture, typically having a distinctive grain size and shape distribution. Extensive work has been carried out to understand the physics of fault rocks, including analysis of natural rocks, laboratory experiments, and theoretical modeling (e.g. Abe and Mair, 2005; Allegre et al., 1982; An and Sammis, 1994; Blenkinsop, 1991; Blenkinsop and Fernandes, 2000; Engelder, 1974; Marone and Scholz, 1989; Sammis et al., 1986, 1987 Sammis and Biegel, 1989; Sammis and King, 2007; and many others). However, quantitative studies of fault rock material to date have mainly focused on considering particle size distributions (PSDs). PSDs give valuable information concerning the size characteristics of an ensemble of particles, but say nothing about the shape of the particles i.e. particles having the same PSD do not necessary show comparable shape characteristics. Particle shape measurements in addition to PSDs may provide a much more effective descriptor of fault rocks and can be easily measured when particle size has been determined. The interplay between particle size and shape influences both the frictional behaviour and porosity and permeability properties of fault zones. However with a few exceptions, notably the recent work by Heilbronner and Keulen (2006) and Storti et al. (2007), particle shape is often ignored (or at least not quantified) in studies of fault rock material.

Somewhat in contrast, grain shape has been viewed as an important and often used descriptor in qualitative and quantitative sedimentology (e.g. Barrett, 1980; Boggs, 1967; Blott and Pye, 2008; Dobkins and Folk, 1970; Folk, 1955; Howard, 1992; Krumbein, 1941; Powers, 1953; Mazzullo and Ritter, 1991; Smith and Cheung, 2005; Wadell, 1936). In this study we show the potential advantages of quantifying PSD, particle shape, and mineralogy for a better understanding of deformation processes.

Textural analysis of fault rock material may yield important constraints on chemical reactions occurring in different mineral phases. Despite the obvious importance of mineralogy, phase differentiation is rarely employed in quantitative studies of fault rock material and instead, the bulk properties of all the fractured material are generally studied together. This is appropriate when

* Corresponding author. Tel.: +47 22 85 64 66; fax: +47 22 85 51 01.
E-mail address: t.e.bjork@fys.uio.no (T.E. Bjørk).
URL: http://www.fys.uio.no/pgp

0191-8141/$ – see front matter © 2009 Elsevier Ltd. All rights reserved.
doi:10.1016/j.jsg.2009.03.020

considering laboratory experiments of mono-mineralogical rocks, where reactions are limited. However, in natural rock when faults and fractures develop and evolve, the system is opened for fluid infiltration. The fluids act as catalysts promoting chemical reactions of specific mineral phases, both as the nucleation of new minerals, and by the growth/decomposition of pre-existing mineral phases (e.g. Antonellini and Aydin, 1994; Chester et al., 1993; Engvik et al., 2005; Morrow et al., 2001; Sibson, 1996; Wintsch et al., 1995).

In this study we use a combination of techniques to highlight characteristic differences and possible different origins of granular material found in fault gouges and clastic dikes, since these features are commonly difficult to distinguish. This includes field observations, classical textural analysis, and the development of a new image analysis technique for quantitative grain characterization.

2. Geological observations

2.1. Geological framework

The rocks studied in this paper are found in the Bremanger Granitoid Complex (BGC), along the Northwestern contact of the Hornelen basin, the largest of three Devonian basins situated in Western Norway (Fig. 1). These basins are related to the Devonian collapse of the Caledonides and have formed as stepwise coarsening to fining upwards sequences of sand, silt, and conglomerate. The basins were formed during late- to post-orogenic extension of the overthickened Caledonian crust and reactivation of the Nordfjord-Sogn Detachment Zone mainly due to a relative change in plate motion between Laurentia and Baltica (Osmundsen and Andersen, 2001). Several studies concerning the general basin development and structural geology in the area have been carried out (e.g. Bryhni, 1978; Steel et al., 1985; Norton, 1986; Seranne and Seguret, 1987; Cuthbert, 1991; Hartz et al., 1994; Andersen, 1998; Osmundsen et al., 1998; Osmundsen and Andersen, 2001; Wilks and Cuthbert, 1994 and references therein).

2.2. Field observations

The BGC is exposed on the Bremanger peninsula and is unconformably overlain by Devonian sandstone sediments along its southern border. Previously this contact has been regarded as an angular unconformity (Bryhni, 1978; Steel et al., 1985; Norton, 1986; Seranne and Seguret, 1987; Wilks and Cuthbert, 1994). However, field work (Hartz et al., 1994; Bjørk, 2006a; Rønjom, 2006) shows that the granodiorite, in the vicinity of the Hornelen basin, is also extensively deformed (see Appendix Detailed geological map). Both ductile and brittle deformation features are observed. The brittle deformation consists of faults, fractures with granulated material, breccias, and clastic dikes filled with basin and wall-rock material. The dominant type of deformation varies with distance from the margin (Table 1). In this study we have quantified the fault gouge (granular debris derived from faulting) and clastic dike structures more closely to gain insights into possible deformation/emplacement mechanisms.

Numerous joints and faults with a NW–SE orientation occur in the granodiorite in the vicinity of the Hornelen basin (Bjørk, 2006a). The general lack of passive markers makes it difficult to quantify displacement along possible faults. However, locally the granodiorite has a strongly developed foliation, with quartz veins parallel to the foliation and the displacement along faults becomes apparent (Fig. 2). Fault sample BRE1505-2 was drilled from the fault marked by a circle (Fig. 2) in locality BRE60-05. Several faults, both sinistral and dextral, are found in this area, with apparent displacements between 1.5 and 18 cm. Over a 10 m long profile oriented approximately perpendicular to the faults, 10 faults are encountered and their accumulated displacement is about 60 cm. The locality is located approximately 150 m away from the contact with the basin (see Appendix Detailed geological map for geographical location).

Immediately adjacent to the margin (up to 5 m) the fracturing is locally so intense that a marginal breccia has formed with orthogonal fractures oriented parallel and perpendicular to the basin margin. The perpendicular fractures terminate at the basin margin. Here, no relative shear displacement along the fractures is observed. Near the basin margin (up to 20 m) fractures 2–3 m long and up to 25 cm thick are found. The majority of the fractures are oriented perpendicular to the basin margin (NW–SE to N–S) and are filled with basin and wall-rock material (Bjørk, 2006a). Several of the fractures near the basin margin are in fact pull-apart fractures (Fig. 3). In the fractures we generally observe flow structures, but granulated material with small clasts of wall-rock material is also observed in some subsidiary connecting fractures. Locality BRE59-05 is approximately 20 m from the basin margin (see Appendix Detailed geological map for geographical location). Two sets of NW–SE oriented fractures filled with brown material exhibiting flow structures are found (Fig. 3) and interpreted as clastic dikes. Dike sample BRE1305A-1 was drilled from the dike shown in Fig. 3.

2.3. Microstructural observations

Samples of the granular material from fault and dike localities described above, were thin sectioned and analyzed using an optical Olympus BX41 microscope and Jeol JSM 6460LV scanning electron microscope. Back scatter electron (BSE)-images with magnifications ranging from 100 to 1500× were taken to study grain size and shape of the fracture infill material. Both thin sections are orientated parallel to strike and perpendicular to the dip directions of the respective fracture structures.

In both samples the wall-rock consists of mainly quartz, plagioclase with radiating epidote needles and K-feldspar, and sericite (Figs. 4 and 6). The wall-rock is intensely fractured in the fault sample, with fractures mainly sub-parallel and sub-normal to the fault zone (Fig. 4). Decomposition of plagioclase is strongest near fractures and the plagioclase, epidote and sericite forms a mesh structure surrounding the larger quartz aggregates. The dike wall-rock shown in the thin section consists of 4 large fragments completely surrounded by fractures and the dike itself. We do not find large centimeter sized fragments in the dike material, but we observe granulation within the fractures of the wall-rock.

In the fault sample, the fault zone mainly consists of an "apparently mylonitic" zone and a very fine-grained gouge zone (Fig. 4). The "apparently mylonitic" zone is banded with dark and light coloured bands. The dark bands consist of mainly epidote. The light coloured bands appear as relatively large grains, but under crossed Nicols we observe that they consist of small fragments of mainly quartz and feldspar with minor amounts of epidote. The "apparently mylonitic" zone was not dealt with using the image analysis tool.

In the gouge zone the grain size distribution appears bimodal at this scale of observation, with mainly a fine-grained matrix and few large survivor grains (matrix supported, large matrix/clast ratio). The matrix consists of all the mineral phases found in the wall-rock and minor amounts of accessory minerals (sericite, titanite and zircon) however, the survivor grains are predominantly quartz. The fault zone is cut by thin light coloured bands of mainly quartz and accessory epidote (Fig. 4). Two generations of these bands which displace each other are observed. On the right hand side of the gouge zone there is a thin transition zone with large fragments of the wall-rock breaking loose from the wall (Fig. 4). The fragments

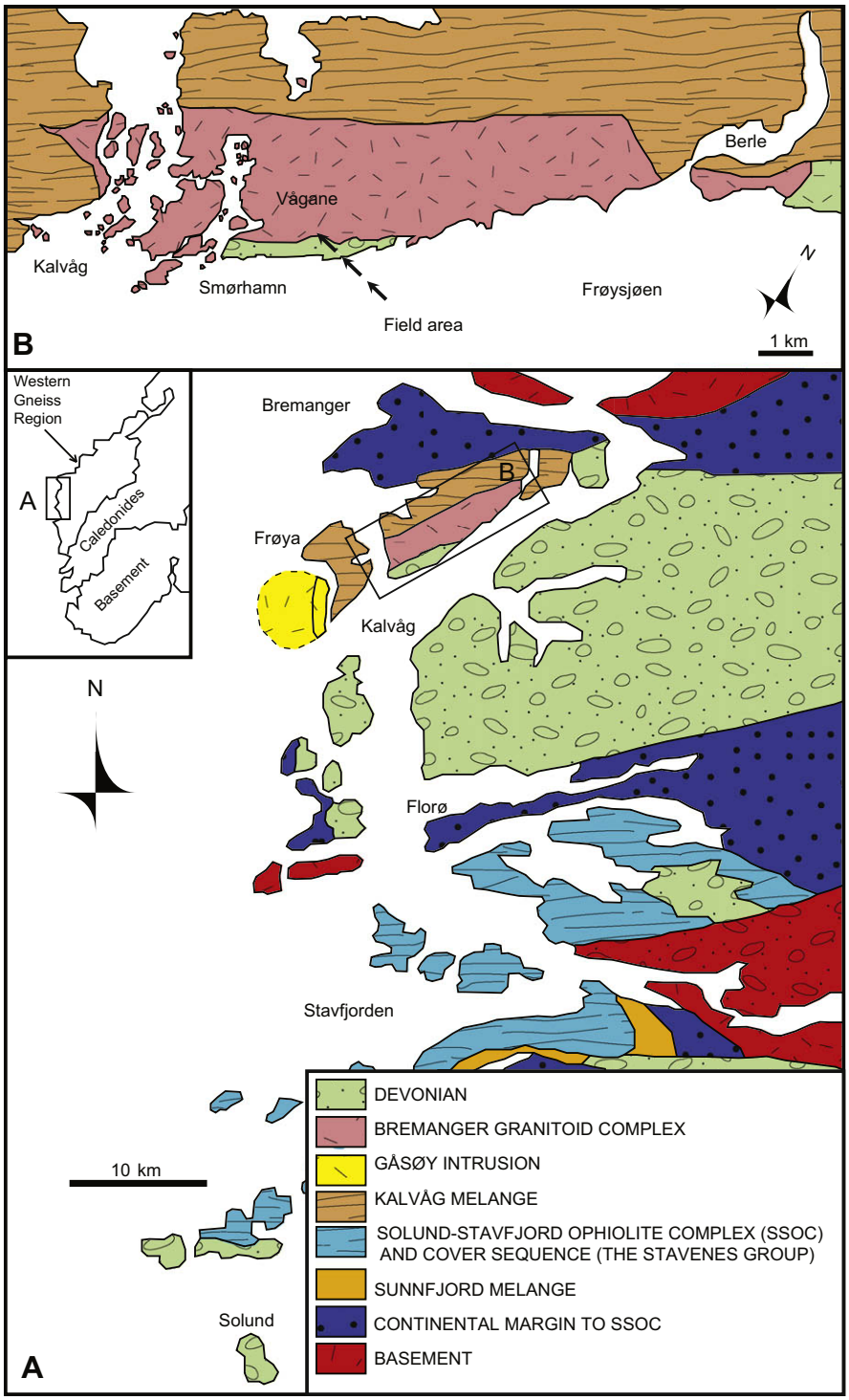

Fig. 1. Simplified map showing the geology of the Solund–Bremanger area in Western Norway (61°33′37.91″N 4°59′45.08″E). The field area (61°47′27.07″N 4°59′55.64″E) was in the BGC near the Northern margin of the Hornelen Basin on the Bremanger-landet peninsula (B). Modified from Hansen et al. (2002) and references therein.

have an elongated shape with their longest axis parallel with the fault in the oriented sections that have been studied. The epidote in the gouge zone displays a complex structure (shown in detail in Fig. 5) that is similar to that of the epidote in the subsidiary fractures in the wall-rock. The epidote grains in the gouge zone are fragmented with irregular shapes, black inclusions of quartz, plagioclase and voids, and zonation with Fe-rich rims. The K-feldspar and plagioclase and quartz grains display an interweaving texture and lobate grain boundaries.

The clastic dike material exists in pull-apart fractures and consists mainly of quartz and epidote of apparently fairly uniform grain size at this scale of observation (Fig. 6). A first order observation is an absence of large "survivor grains". The abundance of the two different phases in the matrix appears homogenously distributed, however inspection of the dike at low magnifications in the thin section reveals the occurrence of light coloured quartz-rich flow bands. Some granulated material also occurs in subsidiary fractures in the wall-rock of the sample (Fig. 6). Epidote appears to

Table 1
Table summarizing the different deformation types with distance from the basin margin. Immediately adjacent to the basin margin (0–5 m) the deformation is locally so intense that a marginal breccia has formed. Near the basin margin (<20 m) clastic dikes (pull-apart fractures) dominate. Up to 600 m away from the basin margin, faults, fault gouges, fractures with granulated material, and breccias are found.

N/NW			S/SW
	Granodiorite		
0 - 400/600 m	0 - 20 m	0 - 5 m	Basin
Faults, fault gouges, fractures with granulated material and breccias	**Clastic dikes (pull-apart fractures)**	**Marginal breccias**	
Fault gouge (150 m): Shear fracture with in-situ granulation of wall-rock material - Large *D*-values - Granulation in fault gouge and wall-rock	Mixed signature Granulation: - Large *D*-values - Granulation in connecting fractures and wall-rock	Perpendicular fractures Extensional fractures filled with basin material	
Mechanism switch: Preferential fracturing along cleavage planes ⇓ Decreasing particle size ⇓ Particle abrasion	Infill of basin material: - Flow structures ⇒Pressurized fluid - Proximity to basin		
Epidote texture: - Fluids from basin - Multiple faulting events	Epidote texture: - Fluids from basin		

be much more abundant in the dike than in the gouge sample (Fig. 7). The epidote grains in the dike display a complex structure (Fig. 7). BSE-images reveal that the epidote grains are fragmented with irregular shapes, black inclusions of quartz, plagioclase and voids. Importantly, the epidote grains in this dike sample lack the concentric growth found in the gouge sample.

3. Quantitative method

To extract quantitative particle size and shape information from images of thin sections a new image analysis tool using MATLAB's Image Processing Toolbox (The MathWorks, 2001) was developed. The program "Gray Scale Image Analysis" (Bjørk, 2006b) uses gray scale-thresholding to separate mineral phases and individual grains. For a more detailed description see Bjørk (2006a) or visit http://folk.uio.no/torbjoeb/image_analysis/. Gray scale BSE-images are read directly into MATLAB. The images are obtained from scanning electron microscope (SEM) studies of the thin sections. The intensity of BSEs is proportional to the atomic mass unit of the element and this phenomenon is used to distinguish the different mineral phases and identify the individual grains (Fig. 8). In this study, three individual mineral phases were differentiated: epidote (E); K-feldspar (K) and plagioclase with quartz (PQ). Sodium-rich plagioclase and quartz have the same intensity range and are difficult to distinguish by this method. It is possible to separate sodium-rich plagioclase and quartz by using the SEM's EDS-analyzer to map the sodium content, however, this is a very time consuming procedure and therefore is not a feasible tool to use on many images. We therefore treated the two as a single phase, even though we recognize that the rheological properties of the two minerals are somewhat different.

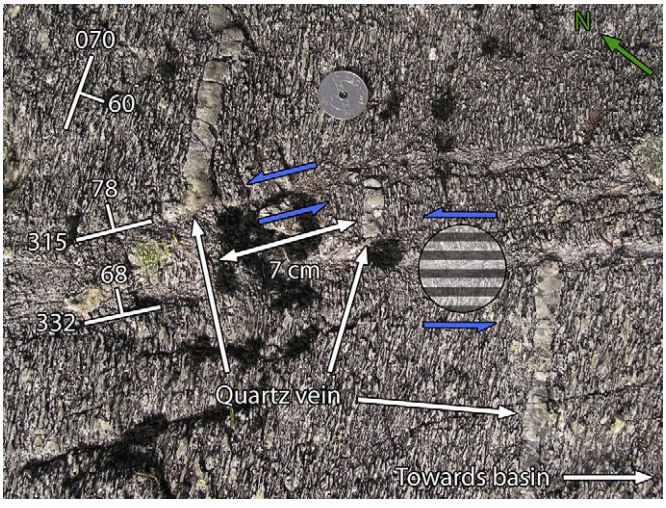

Fig. 2. Fault locality. The locality is approximately 150 m away from the basin margin. The right hand side of the image is pointing towards the basin margin. The granodiorite has a strongly developed foliation and the apparent offset becomes visible from the displaced quartz vein. Sample BRE1505-2 was drilled from the fault marked with the circle. Coin for scale is ~21 mm in diameter.

When the appropriate gray scale range is found for a phase of interest, the image is thresholded and turned into a binary image for that phase with the grains set to 1 and the background set to 0 (Fig. 8). Several morphological operations are applied to further separate the individual grains. All morphological operations inspect the pixels in a 3×3 pixel-environment. First, image noise due to overlapping gray scale intensities of different mineral phases is reduced by removing isolated white pixels. To separate any joined grains, H-bridges and spurs are removed and morphological opening (erosion followed by a dilation) is performed once or several times. Finally, inclusions within the grains are filled. To limit the minimum grain size detectable on each magnification image (i.e. remove matrix), all grains with an area less than 200 pixels are removed. This is a reasonable limit for high resolution images, since smaller matrix thresholds would add error to calculations of particle shape. Grains that touch the edges of the image are removed and their area is subtracted from the total area of the processed image since their entire size and shape are unknown. The image is then labeled using nearest neighbour connectivity with the connecting white pixels (i.e. grains) given a positive integer value while the background remains set to 0. From the resulting labeled image, the size and shape properties (and orientations) of the grains can easily be calculated.

The success of the image processing technique relies predominantly on the contrast and the resolution of the image. If the contrast between particles and matrix, or different phases is small, they will not be properly differentiated. The best results are

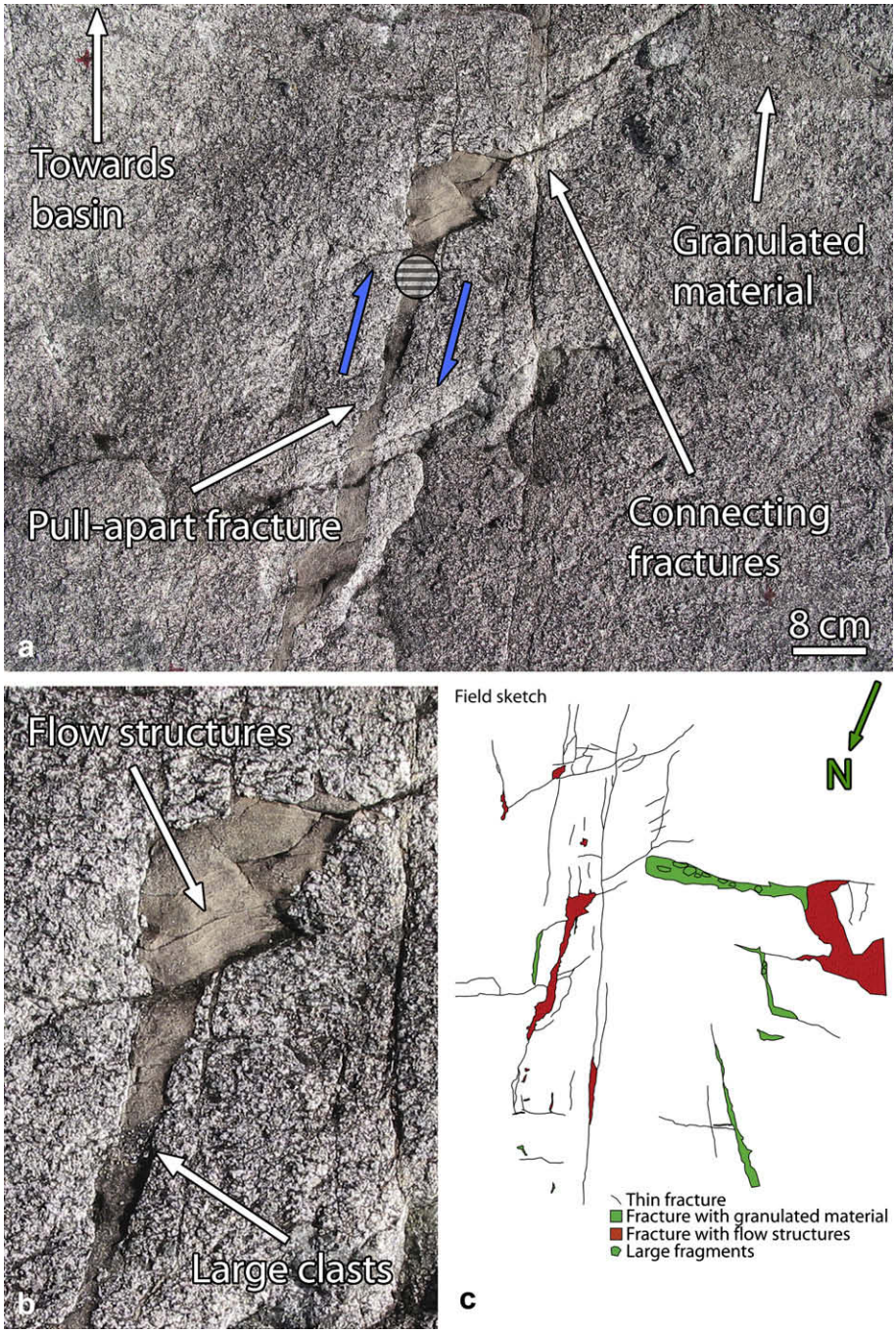

Fig. 3. Dike locality. The locality is approximately 20 m away from the basin margin. a) The top of the image is pointing towards the basin. The main fractures are oriented 158/71, approximately perpendicular to the basin margin. Sample BRE1305A-1 was drilled from a pull-apart fracture on the left marked with a circle. The shear displacement is approximately 10 cm. Notice that the pull-apart fracture is connected with parallel fractures and areas with granulated material in the top right corner. b) Close-up of pull-apart dike sample in a). Flow structures and occasional large clasts are observed in the field (shown by arrows). c) Field sketch of the locality.

obtained for high resolution images which allow easy phase differentiation and particle separation, and require minimal morphological operations that can alter particle size and shape. Identification of the individual grains is relatively easy when the sample material consists of isolated grains of the same mineral phase or grains with nearly touching boundaries. When grains of the same mineral phase have a long connecting grain boundary, the grain separation becomes more difficult and typically requires more advanced processing. Excessive morphological opening and closing should be avoided, because it imposes the geometric structure of the structuring element onto the particles. Hence, to avoid these unwanted artifacts, prior to processing in MATLAB, the grains of a single mineral phase that have long connected grain boundaries have been separated manually using Adobe Photoshop. Other potential issues include: i) accessory minerals that may be wrongly identified as grains of one of the principal mineral phases and must be removed manually; and ii) overlapping gray scale intensities that will add noise to the image, however this is avoided by the removal of any isolated white pixels and connected pixels smaller than the limit for the minimum grain size detectable.

The main advantage of this method over other image tools is that it is not a "black box method". The script is written in native

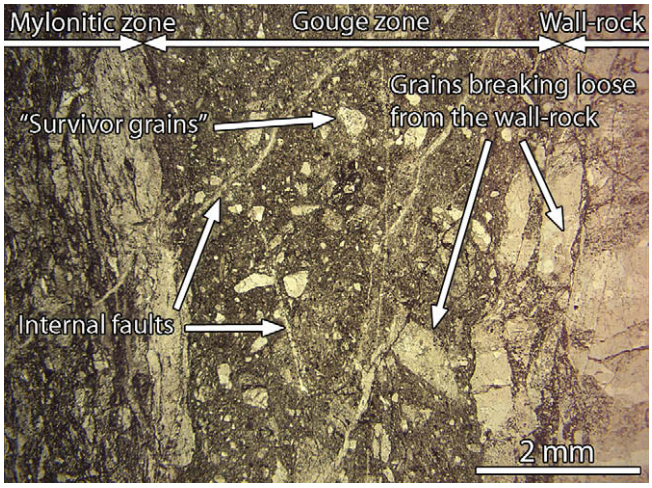

Fig. 4. Transmitted light (TL)-image of the fault sample. The wall-rock is highly fragmented sub-parallel and sub-normal to the fault. The wall-rock consists of relatively large aggregates of quartz grains and small grains of plagioclase that have partly or completely decomposed to epidote and chlorite. Transition zone on the right consists of relatively large fragments breaking loose from the wall-rock. The gouge material has a fine-grained matrix and a few large survivor grains. The gouge zone is cut by two light coloured quartz bands interpreted as "internal faults" formed after the gouge material had lithified. The "mylonitic" zone on the left is banded with dark (epidote-rich) and light coloured bands (consisting of small fragments of mainly quartz, feldspar and minor epidote).

MATLAB which makes it adaptive and user-friendly for non-programmers. In contrast to most available closed-source programs, the MATLAB script allows full user access to view and modify the inbuilt functions used to separate phases and identify grains. This leads to a better understanding of how these operations affect the resulting particle size and shape. Furthermore, it is very easy to tune the settings, for various types of images, and statistical treatment and data visualization are conveniently available in the same package.

The program "Gray Scale Image Analysis" (Bjørk, 2006b) is designed to be semi-automatic and requires minimal user-input, however, a vital stage is the user evaluation of the image processing. A key benefit of this tool is that it allows graphical evaluation of the result. Image analysis is not failsafe, therefore efficient evaluation or quality control of the image processing is essential to check for accurate identification of phases, any misfit of grain boundaries or any overlap between phases. To evaluate the quality of the grain identification, the boundaries and centroids of the identified individual particles are superimposed onto the original unaltered BSE-image (Fig. 8). Particle overlap, for example, will be clearly visible when the image of all the phases combined is displayed and colour-mapped and can then be manually corrected.

Although, some manual adjustments are inevitable for optimization of individual images, this image tool can successfully differentiate different phases and detect individual grains with minimal user-input. We believe this approach provides a very good approximation of particle size, shape, and orientation, in a relatively short time, provided that the overlay of detected grain boundaries match the original image as highlighted above (Fig. 8).

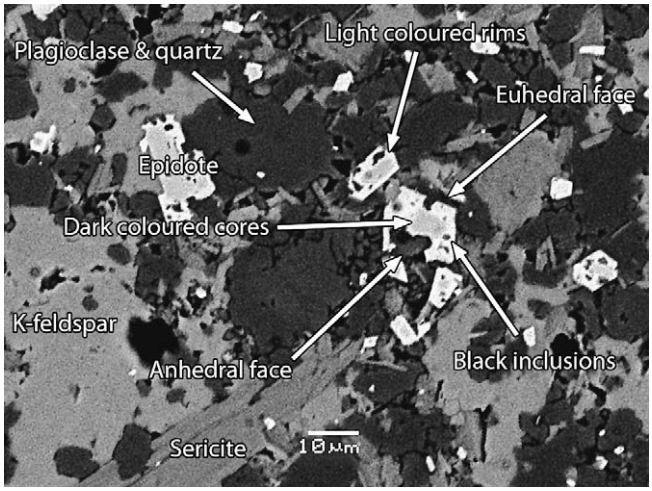

Fig. 5. BSE-image of the gouge zone in the fault sample. The K-feldspar and plagioclase/quartz grains display an interweaving texture and lobate grain boundaries. The epidote grains in the gouge zone display a complex texture with black inclusions of quarts, plagioclase and voids, zonation and fragmented appearance with both well developed and irregular crystal faces. The zonation is due to different amounts of iron.

4. Results

We now present quantitative analyses of grain characteristics, including the relative abundances of different phases, particle size distributions, and particle shape for the fault gouge and clastic dike samples using the image analysis method described above.

4.1. Relative abundance of different phases

In the gouge sample, the most abundant mineral phase is plagioclase/quartz (Table 2), both in terms of number of particles and relative porphyroclast proportion (i.e. area percentage of particles). Approximately 45% of the particles are plagioclase/quartz, ~38% are K-feldspar, and only ~17% are epidote. The porphyroclast proportion for all of the phases combined and the individual phases varies non-linearly with magnification. The relative porphyroclast proportion of epidote increases systematically with higher magnifications.

In the dike sample, plagioclase/quartz is also the most abundant phase (Table 3). Of the total 948 particles, ~42% are plagioclase/quartz, ~38% are epidote, and ~20% are K-feldspar. The porphyroclast proportion of all the phases combined increases with magnification. K-feldspar is the least abundant phase at all magnifications. Plagioclase/quartz dominates at low magnifications, whereas epidote dominates at high magnifications.

4.2. Particle size distributions

Determining the size of a regular shaped particle, e.g. a sphere, is simple since it is uniquely defined by its diameter. However, for cross-sections of irregular shaped particles, size depends on the way it is defined. The most commonly used measurement of particle size is equal area diameter, i.e. the diameter of a circle having the same area as the projected particle (Brittain, 2001). This is a useful derived measurement since it is a single number that gets larger or smaller as the particle does and its measurement is objective and repeatable. Particle size data obtained from image analysis for the gouge sample and dike sample in this paper are presented as equal area diameter (unless otherwise stated).

4.2.1. Gouge sample

In the gouge sample, K-feldspar, and plagioclase/quartz have particles ranging from 2 μm to 190 μm and 410 μm, respectively (Table 2), whereas epidote only exists as relatively small particles (between ~2 and ~90 μm). Grain size distributions by number are presented as cumulative frequency (greater than a given size) normalized to area and displayed on a log–log plot for a range of magnifications (Fig. 9). Data are compared for the bulk sample (i.e. all phases combined) and the individual phases. We suggest that

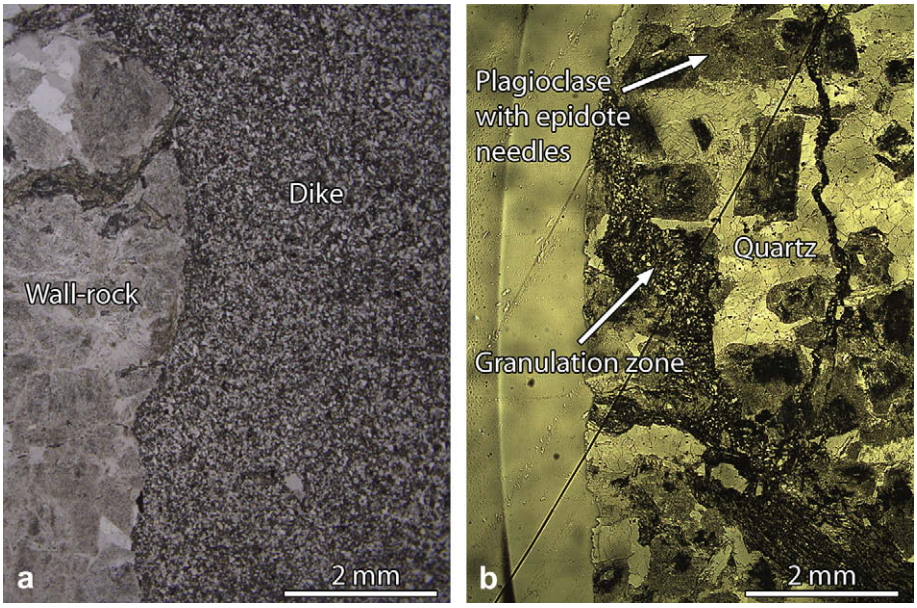

Fig. 6. TL-image of the clastic dike sample. a) The dike material appears at this magnification to be fairly homogenous. We also notice that the interface between the wall-rock and dike is sharp and distinct. b) The wall-rock consists of mainly quartz, plagioclase with epidote needles and K-feldspar, and accessory sericite and chlorite. The plagioclase is partially decomposed to epidote. The epidote phase appears as radiating needles in the cores of the plagioclase. We also find small regions where chlorite dominates the mineral phase assemblage in the wall-rock. Although the wall in the dike sample is not intensely deformed, we observe occasional granulation zones.

the data can be fitted reasonably well, for certain size ranges, by a straight line of slope D. This indicates that the size distribution approximates a power law with exponent D. Note that we now quote a 3-dimensional D-value by adding 1 to our 2-dimensional measurement. We employ this standard technique to allow easy comparison of our data to other published work.

The gouge sample has D-values of ~2.9–3.2 for the majority of the particle size range (denoted D_1) (Table 2 and Fig. 9). For all of the phases combined the D_1-value is 2.9977. Similar D_1-values and ranges are observed for K-feldspar and plagioclase/quartz. However, in all cases the largest fraction of the particles is best fitted with a larger slope D_2 (Table 2 and Fig. 9). Importantly, K-feldspar and plagioclase/quartz phase show similar PSD characteristics which in turn strongly influences the PSD characteristics of all of the phases combined. Unfortunately, this completely masks the PSD characteristics of epidote, the minor phase. Epidote has a higher D_1-value of 3.2323 and a relatively small upper grain size limit of ~60 μm (Fig. 9). In contrast to the other phases, the smallest fraction of epidote grains can be fit with a smaller D_2-value of 1.8020. Hence it is crucial to use phase discrimination to get a true PSD evaluation of the minor phase.

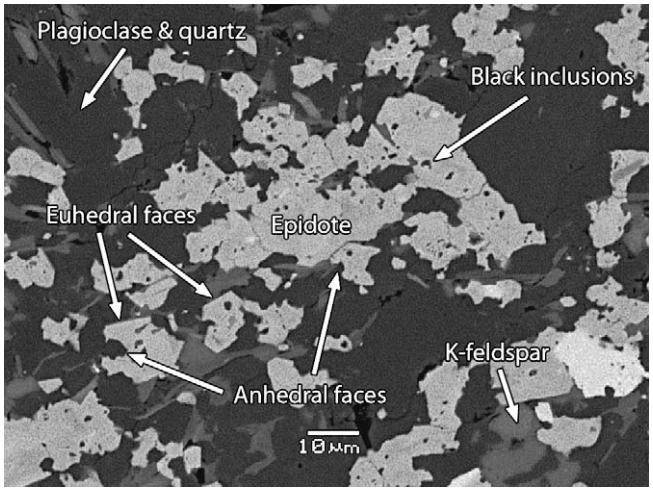

Fig. 7. BSE-image of the clastic dike sample. The K-feldspar and plagioclase/quartz appear as separate grains and do not exhibit an interweaving texture. The epidote grains in the dike display a complex structure. They are fragmented with partly well developed and irregular crystal faces, black inclusions of quartz, plagioclase and voids. However, they show no evidence of concentric growth.

4.2.2. Dike sample

Particle size distributions of the dike sample are plotted by number in Fig. 10 and shown in Table 3. The data are reasonably well fitted by a slope with D-value of 3.2139 for all phases combined. Plagioclase/quartz has the smallest D-value of the individual phases, 2.6673, whereas epidote and K-feldspar have larger D-values closer to that of all the phases combined. K-feldspar has a D-value of 3.0203 and epidote has a D-value of 3.2616. In the dike sample, epidote, and plagioclase/quartz have particles ranging from ~0.6 μm to ~100 μm (Table 2), whereas K-feldspar has an upper particle size boundary of ~65 μm. It is important to note that here the size characteristics of all the phases combined are not particularly representative for the individual mineral phases.

4.3. Particle shape

There are several different ways of quantitatively describing the shape of a particle depending on the aspect of interest. In general it should obey three criteria (Crompton, 2005): (i) It should be intuitive; (ii) it should be normalized to values between zero and 1, thus making interpretation easier; and (iii) it should be sensitive to deviations. It is unlikely that a single shape descriptor can perfectly discriminate and characterize all applications and different combinations of shapes. Hence in this study two different shape parameters, convexity and circularity have been chosen. In the samples analyzed in this study, the orientation of the major axis of grains showed no preferred orientation.

4.3.1. Convexity

Convexity (equivalent to the PARIS factor used by Herwegh et al. (2005)) is a measurement of surface roughness and is calculated by

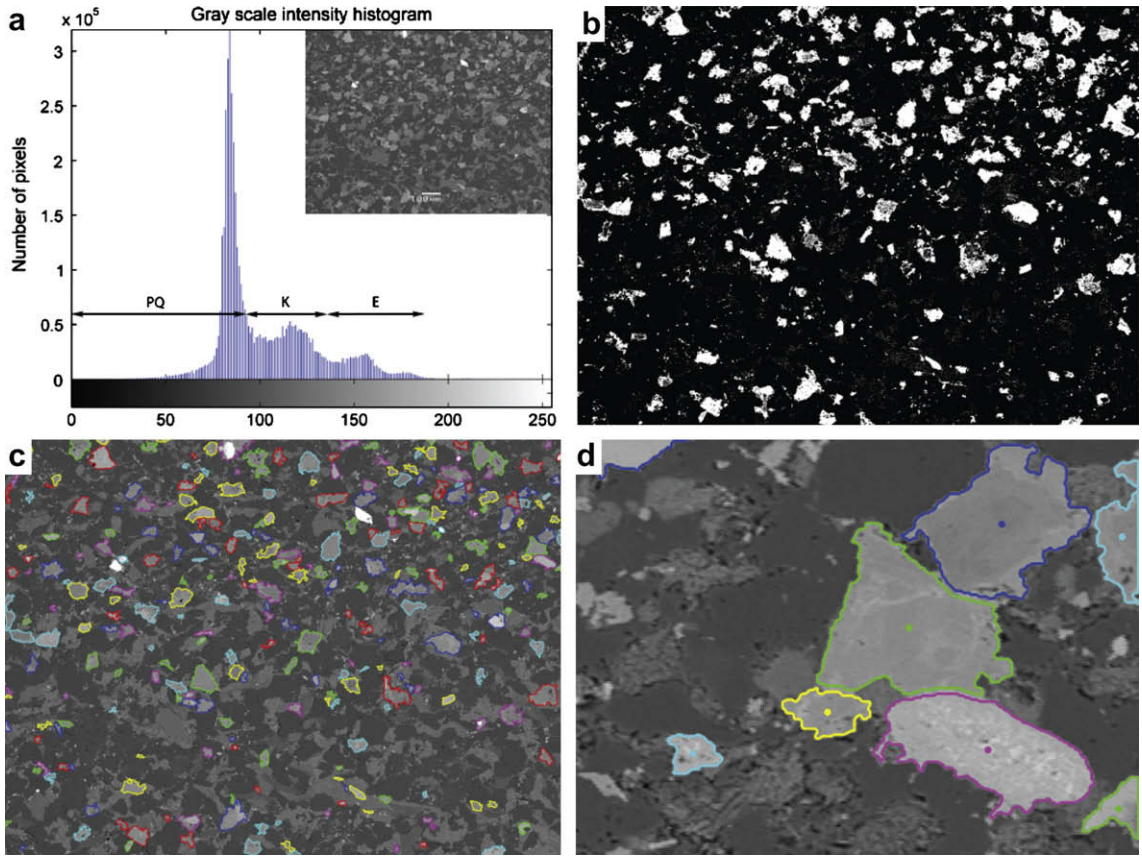

Fig. 8. Evolution and evaluation of mineral phase differentiation and grain identification. a) Histogram of gray scale intensity (0–255) indicating the manual phase separation of epidote (E), K-feldspar (K) and plagioclase/quartz (PQ) based on gray scale intensity. The insert shows the original BSE-image of the dike sample. b) Thresholded binary BW image for the epidote phase. c) Epidote boundaries superimposed onto the original image for comparison using random colours after identification of individual grains. d) Close-up of c) showing the superimposed grain boundaries and centroids of the grains.

dividing the convex hull perimeter (P_{CH}) by the actual particle perimeter ($P_{Particle}$) (equation (1)).

$$\zeta = \frac{P_{CH}^2}{P_{Particle}^2} \quad (1)$$

The convex hull is the smallest convex polygon that can contain the particle. It is best visualized by the area enclosed by an elastic band stretched around the particle. Convexity has values in the range of 0–1, a smooth particle having convexity equal to 1, whereas an irregular particle has convexity closer to 0 (Fig. 11). The convexity is only affected by surface roughness and is unaffected by overall form and symmetry.

4.3.2. Circularity

Circularity is a measure of the ratio of the perimeter of an equal area circle (P_{EAC}) and the perimeter of the actual particle ($P_{Particle}$) (equation (2)).

$$\psi = \frac{P_{EAC}^2}{P_{Particle}^2} = \frac{4\pi A_{Particle}}{P_{Particle}^2} \quad (2)$$

As the name suggests, circularity is a measure of how close the particle shape is to a circle (Fig. 11). Circularity also has values between 0 and 1, a circle having circularity 1, whereas irregular objects have circularity closer to 0. Circularity is sensitive to both overall shape and symmetry, and surface roughness. In order to optimize the convexity and circularity descriptors for subtle variations in shape, squared terms are used in the numerator and denominator of these descriptors, as shown in equations (1) and (2). The perimeter is calculated as the sum of the Euclidean distance between the boundary pixels and the area is calculated as the number of pixels occupied by the particle. Both perimeter and area are scaled to the appropriate BSE-image scale. Particle shape data are now presented as convexity and circularity versus size for epidote, K-feldspar and, plagioclase/quartz, respectively.

4.3.3. Gouge sample

There is a general trend in the gouge sample (observed in all three mineral phases) for a reduction in convexity and circularity with increasing grain size (Fig. 12). This indicates that generally, small grains are smooth and spherical whereas larger grains are rougher and non-circular. Despite the epidote grains being limited to grain smaller ~100 μm, a similar shape and size relationship is observed. One subtle difference in phases is that convexity and circularity for epidote are more evenly distributed throughout the range, whereas for K-feldspar and plagioclase/quartz the convexity values are skewered towards the maximum value. Also notable is that K-feldspar and plagioclase/quartz phases contain large particles interpreted to be "survivor grains".

This subtle difference is also reflected in the convexity characteristics over the entire particle size range (Table 4). The mean values of K-feldspar and plagioclase/quartz are large at approximately ~0.9, while epidote has a lower mean value of ~0.7. The minimum values are low for all phases (~0.2–0.3) and the spread is relatively high (~0.15–0.20). However, the most significant

Table 2
Particle size data from gouge sample BRE1505-2. Porphyroclast proportion and relative porphyroclast proportion are modal area percentage. Small/large fraction is used for the fraction of particles that does not fit the slope D_1 for the majority of the particle size range.

	Gouge sample								
	Porphyroclast proportion (%)							Number of particles	
Magnification	100x	200x	400x	600x	800x	1000x	1500x		
Epidote	1.65	2.97	5.01	6.17	4.97	6.25	12.26	265	17.30%
K-feldspar	8.09	19.71	20.92	29.47	13.20	11.78	7.98	581	37.92%
Plag./quartz	25.60	27.52	30.59	35.58	35.65	35.65	40.49	686	44.78%
Combined	35.34	50.20	56.52	71.22	53.81	53.67	60.74	1532	100.00%
Matrix	64.66	49.80	43.48	28.78	46.19	46.33	39.26		
	100.00	100.00	100.00	100.00	100.00	100.00	100.00		
	Relative porphyroclast proportion (%)								
Magnification	100x	200x	400x	600x	800x	1000x	1500x		
Epidote	4.67	5.92	8.86	8.66	9.23	11.64	20.19		
K-feldspar	22.89	39.26	37.01	41.38	24.53	21.94	13.14		
Plag./quartz	72.44	54.82	54.12	49.96	66.24	66.41	66.67		
	100.00	100.00	100.00	100.00	100.00	100.00	100.00		
Phases	Particle size (diameter $_{EAC}$, μm)					Power-law coefficient, D		Range (μm)	
	Mean	Peak	Min.	Max.				Lower	Upper
Epidote	19.70	15.58	2.27	92.72		3.2323		3.52	59.36
Small fraction						1.8020		2.26	11.57
K-feldspar	29.89	3.28	2.42	190.48		2.9998		4.46	120.3
Large fraction						4.1209		38.68	315.0
Plag./quartz	42.24	3.82, 4.43	3.07	410.22		2.8644		4.43	110.1
Large fraction						3.3477		24.47	260.9
Combined	33.65	8.01	2.26	410.22		2.9977		3.07	115.6
Large fraction						3.7111		29.06	254.0

difference is the skewness and kurtosis. Both K-feldspar and plagioclase/quartz have a long left tails with magnitude $\sim|1.6|$ and "peaked" distributions (kurtosis $\sim$5.1). As opposed to epidote which is more symmetric (skewness ~ -0.4) with a lower kurtosis ($\sim$2.1) giving it a less "peaked" distribution.

We observe the same subtle difference for circularity. K-feldspar and plagioclase/quartz have relatively large mean values ($\sim$0.6–0.65, respectively) (Table 4). They are left-skewed with relatively a long left tail ($\sim|0.7-0.8|$), and the kurtosis is similar to that of a normal distribution ($\sim$3.0). Epidote has a smaller mean value ($\sim$0.5), is more symmetric (skewness ~ -0.10), and a more "flat" distribution with relatively thin tails (kurtosis $\sim$2.0). The minimum values are low for all phases ($\sim$0.10–0.15) and the spread is relatively high ($\sim$0.20).

4.3.4. Dike sample

The dike sample lacks the presence of "survivor grains" and the upper grain size is limited to $\sim$100 μm (Fig. 12). The maximum values of both convexity and circularity of all mineral phases decrease with increasing particle size, although the size–shape relationship is less strong than in the gouge sample. Also noticeable

Table 3
Particle size data of the dike sample BRE1305A1. Porphyroclast proportion and relative porphyroclast proportion are modal area percentage. Small/large fraction is used for the fraction of particles that does not fit the slope D_1 for the majority of the particle size range.

	Dike sample								
	Porphyroclast proportion (%)							Number of particles	
	100x	200x	400x	600x	800x	1000x	1500x		
Epidote	7.14	11.86	21.21	25.11	21.15	50.77	61.24	361	38.1%
K-feldspar	6.03	3.75	3.29	6.60	8.97	5.78	8.57	187	19.7%
Plag./quartz	15.00	26.04	36.47	26.92	25.03	13.28	9.91	400	42.2%
Combined	28.17	41.66	60.97	58.63	55.15	69.83	79.72	948	100%
Matrix	71.83	58.35	39.03	41.37	44.85	30.17	20.28		
	100.00	100.00	100.00	100.00	100.00	100.00	100.00		
	Relative porphyroclast proportion (%)								
	100x	200x	400x	600x	800x	1000x	1500x		
Epidote	25.35	28.48	34.79	42.83	38.35	72.71	76.82		
K-feldspar	21.41	9.00	5.40	11.26	16.26	8.28	10.75		
Plag./quartz	53.25	62.52	59.82	45.92	45.39	19.02	12.43		
	100.00	100.00	100.00	100.00	100.00	100.00	100.00		
Phases	Particle size (diameter $_{EAC}$, μm)					Power-law coefficient, D		Range (μm)	
	Mean	Peak	Min.	Max.				Lower	Upper
Epidote	17.32	8.06	3.00	95.96		3.2316		4.43	58.47
K-feldspar	17.87	4.01	2.21	65.48		3.0203		3.28	43.95
Plag./quartz	22.73	36.96	0.56	108.75		2.6673		2.48	72.55
Combined	19.71	7.61	0.56	108.75		3.2139		3.86	69.16

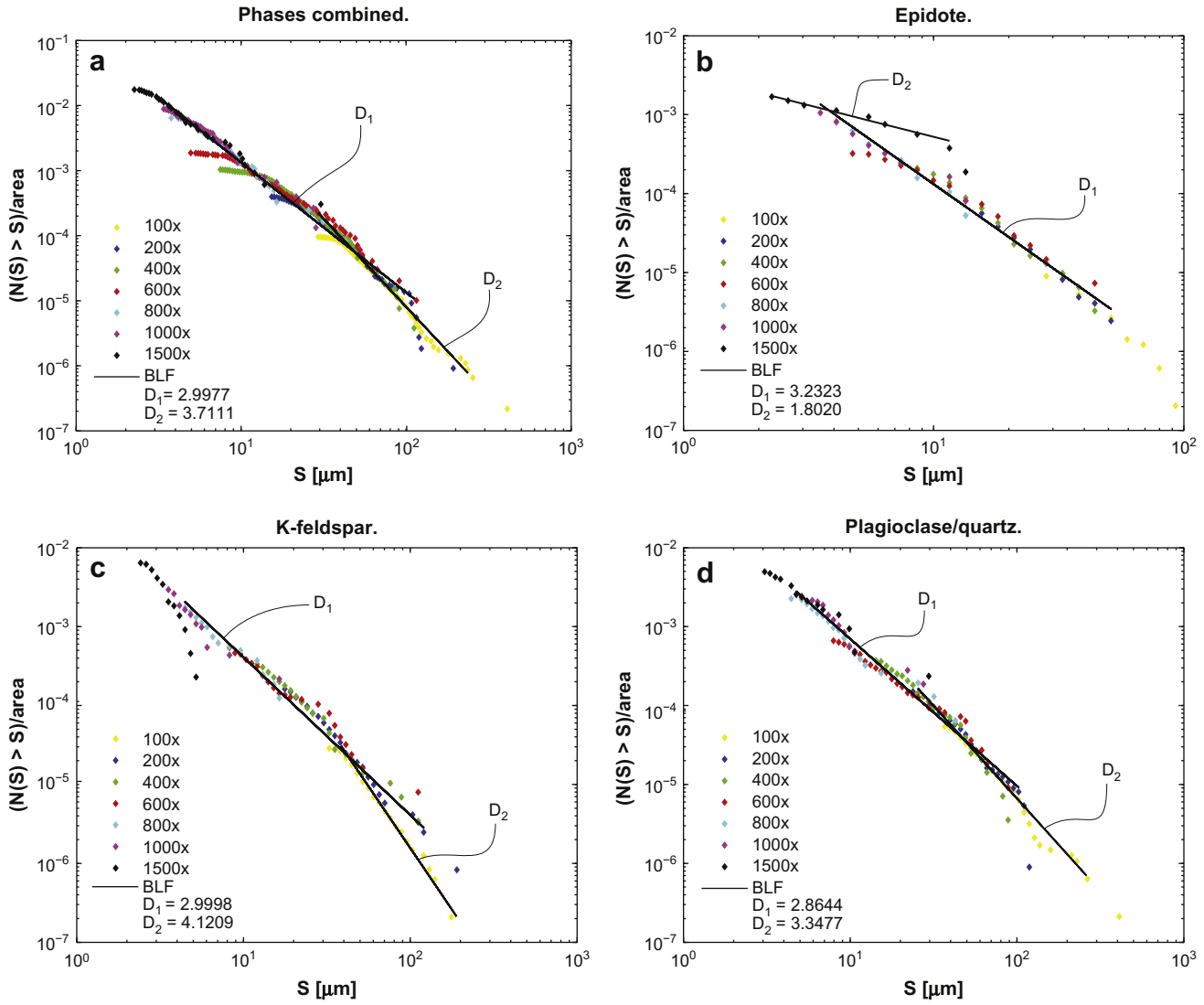

Fig. 9. PSD of the gouge sample presented as cumulative frequency (greater than a given size) normalized to area and displayed on a log–log plot for a range of magnifications 100–1500× a) phases combined, b) epidote, c) K-feldspar, and d) plagioclase/quartz). The gouge sample has a slope D_1 for the majority of the particle size range but a slope D_2 better fits the largest or smallest size fractions. The gouge sample has low D_1-values ranging from ~2.9 to ~3.2 for plagioclase/quartz, K-feldspar, and epidote, respectively. The D_1-value is ~3.0 for all the phases combined. K-feldspar, plagioclase/quartz, and all of the phases combined the largest fraction of particles have D_2-values between ~3.3 and 4.1. In contrast, the smallest fraction of epidote grains can be fit with a smaller D_2-value of ~1.8. See text for discussion of D-values.

is that throughout the particle size range, the convexity values of all the phases in the dike sample are skewed towards the maximum value. Whereas for circularity the values are more evenly distributed throughout the particle size range.

Over the entire particle size range, all the individual phases have mean values of ~0.9 for convexity (Table 4). All of the phases are left-skewed, however, epidote and K-feldspar have relatively lower magnitudes of ~|1.1|, whereas plagioclase/quartz has a larger magnitude of ~|1.7|. All the distributions are leptokurtic (i.e. kurtosis > 3), but epidote and K-feldspar have relatively small kurtosis values of ~3.6–3.8. Plagioclase/quartz has a large kurtosis value of ~5.7 resulting in a more distinct peak. The minimum values are generally relatively high (compared to the gouge sample) for all phases (~0.3–0.4) and the spread is around 0.12–0.13.

For circularity, the individual phases have similar mean values and spread of ~0.8 ± 0.1 (Table 4). All the phases are left-skewed. Epidote and plagioclase/quartz have skewness of ~ −0.6 and ~ −0.9, respectively, while K-feldspar is slightly more centered around its mean value (skewness ~ −0.4). Similarly epidote and plagioclase/quartz have kurtosis values of ~2.7 and ~3.0, respectively, close to that of a normal distribution. K-feldspar has a slightly lower kurtosis value of ~2.5. The minimum values are relatively high (compared to the gouge sample) for all phases (~0.4–0.45).

5. Discussion

5.1. Overview

On considering the D-values for the bulk material (i.e. all phases combined) and interpreting consistently with previous work (Marone and Scholz, 1989; Blenkinsop, 1991; An and Sammis, 1994; Blenkinsop and Fernandes, 2000; Storti et al., 2003; Heilbronner and Keulen, 2006), it would appear that the dike has a more evolved (or mature) size distribution texture than the gouge sample (Tables 2 and 3). The two samples show distinct field and textural characteristics, porphyroclast content, and importantly, the grain size and shape distributions of the individual phases are distinct.

In the gouge sample, K-feldspar and plagioclase/quartz are the main constituents of the porphyroclasts (Table 2). They generally show similar size–shape characteristics (Fig. 13). Epidote, the minor

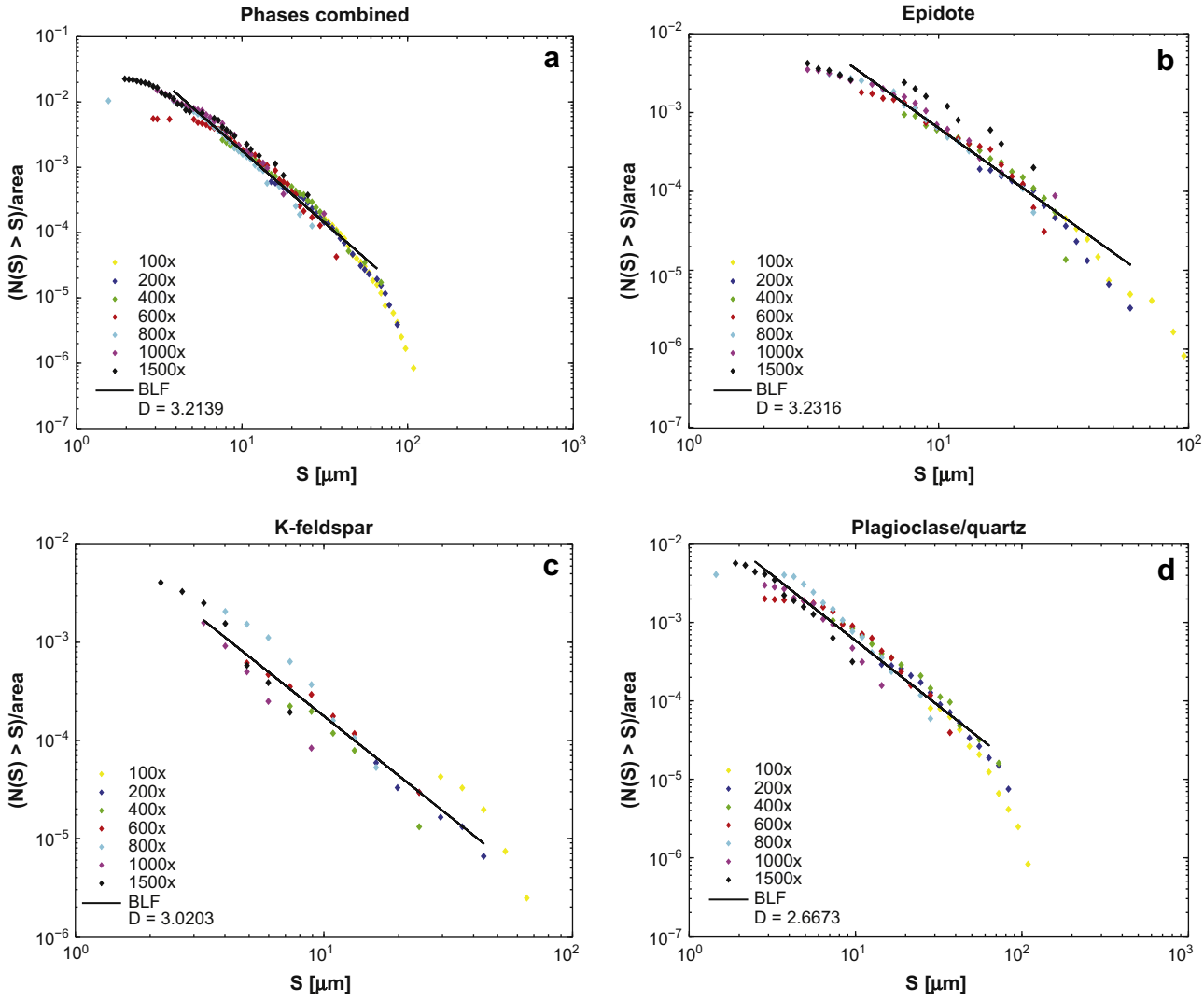

Fig. 10. PSD of the dike sample presented as cumulative frequency (greater than a given size) normalized to area and displayed on a log–log plot for a range of magnifications 100–1500×. The dike has high *D*-values ranging from ~2.7 to ~3.2 for plagioclase/quartz, K-feldspar, and epidote, respectively. The *D*-value is ~3.2 for all the phases combined.

porphyroclast constituent shows different characteristics, but importantly, this is masked by the other phases when data for all the phases combined are evaluated.

In contrast, for the dike sample, size and shape characteristics are distinct for different mineral phases. Epidote (more abundant here) and K-feldspar (the least abundant phase) have similar size characteristics in that $D \geqq 3.0$ (Table 3). Plagioclase/quartz dominates the porphyroclast assemblage at low magnifications, while epidote is most abundant at high magnifications.

5.2. Insights into fragmentation processes from shape characteristics

In the gouge sample, K-feldspar and plagioclase/quartz show a negative relationship between size and shape, with smaller grains being more circular and smoother which saturates to a value of 1 at small sizes (Fig. 13). Intragranular fragmentation will create irregular and non-spherical grains, whereas particle abrasion would yield smaller, smooth particles that become progressively more spherical. This may indicate, in our samples, that with increasing granulation and size reduction (presumably associated with increased fault maturity), preferred fracturing along cleavage planes is reduced and the grains are rather abraded or crushed, thus, creating small spherical grains with a smooth surface. Hence, we suggest that both preferential intragranular fragmentation of larger K-feldspar and plagioclase/quartz grains (Blenkinsop, 1991; Blenkinsop and Fernandes, 2000) and particle abrasion (Hattori and Yamamoto, 1999; Storti et al., 2003) have been active during faulting. This apparent switch in deformation mechanism may

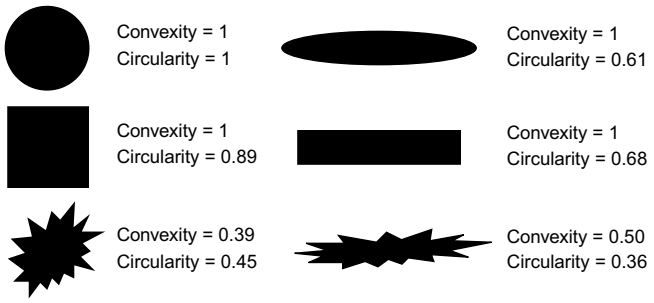

Fig. 11. Two different shape parameters, convexity and circularity, have been chosen to discriminate and characterize the particle shapes. Examples of convexity and circularity values for different shapes are illustrated above. Note that convexity is unaffected by overall form and symmetry, while circularity is sensitive to both overall shape and symmetry. Modified from Crompton (2005).

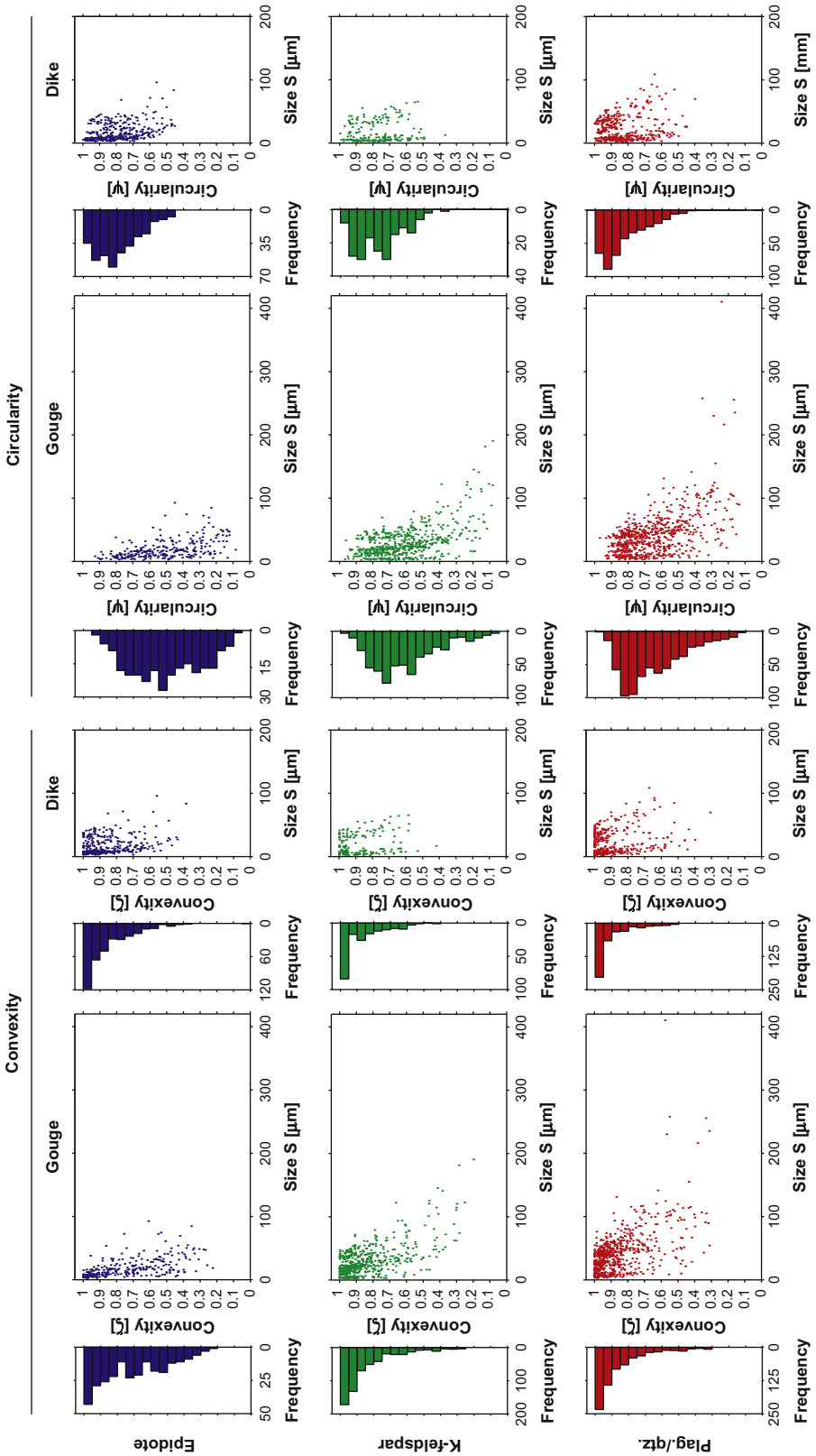

Fig. 12. Scatter plots of convexity, and circularity versus size (equal area diameter) and histograms illustrating the shape characteristics for the individual mineralogical phases in the two samples.

explain the *D*-values larger than 3. This has also been suggested by Storti et al. (2003) and Keulen et al. (2007).

In contrast, the non-diagenetic phases in the dike sample (i.e. those who have not grown from fluid-rock interaction) show an absence of any strong size–shape relationship and in spite of the relatively large *D*-values, have a distinct lack of the large "survivor grains" typically found in fault gouges (Fig. 13). "Survivor grains" of epidote are absent in both samples, however, this is unsurprising

Table 4
Table summarizing shape characteristics of samples BRE1505-2 (gouge) and BRE1305A1 (dike). The peak values are taken from the his-tograms in figure 12.

		Convexity							
		Max.	Min.	Mean	Med.	Std.	Peak	Skewn.	Kurt.
Epidote	Gouge	1.00	0.23	0.73	0.75	0.20	0.95	−0.43	2.09
	Dike	1.00	0.39	0.86	0.91	0.13	0.95	−1.14	3.75
K-feldspar	Gouge	1.00	0.20	0.85	0.91	0.16	0.95	−1.58	5.13
	Dike	1.00	0.42	0.88	0.91	0.12	0.95	−1.10	3.56
Plag./qtz.	Gouge	1.00	0.31	0.86	0.91	0.15	0.95	−1.59	5.13
	Dike	1.00	0.31	0.90	0.95	0.13	1.00	−1.73	5.71
		Circularity							
		Max.	Min.	Mean	Med.	Std.	Peak	Skewn.	Kurt.
Epidote	Gouge	0.93	0.09	0.51	0.52	0.20	0.53	−0.07	2.06
	Dike	1.00	0.45	0.80	0.82	0.13	0.84	−0.58	2.68
K-feldspar	Gouge	0.97	0.08	0.62	0.65	0.19	0.74	−0.67	2.95
	Dike	1.00	0.37	0.77	0.78	0.13	0.74/0.79	−0.40	2.48
Plag./qtz.	Gouge	0.97	0.14	0.65	0.69	0.18	0.79	−0.75	2.86
	Dike	1.00	0.40	0.83	0.87	0.13	0.95	−0.91	3.09

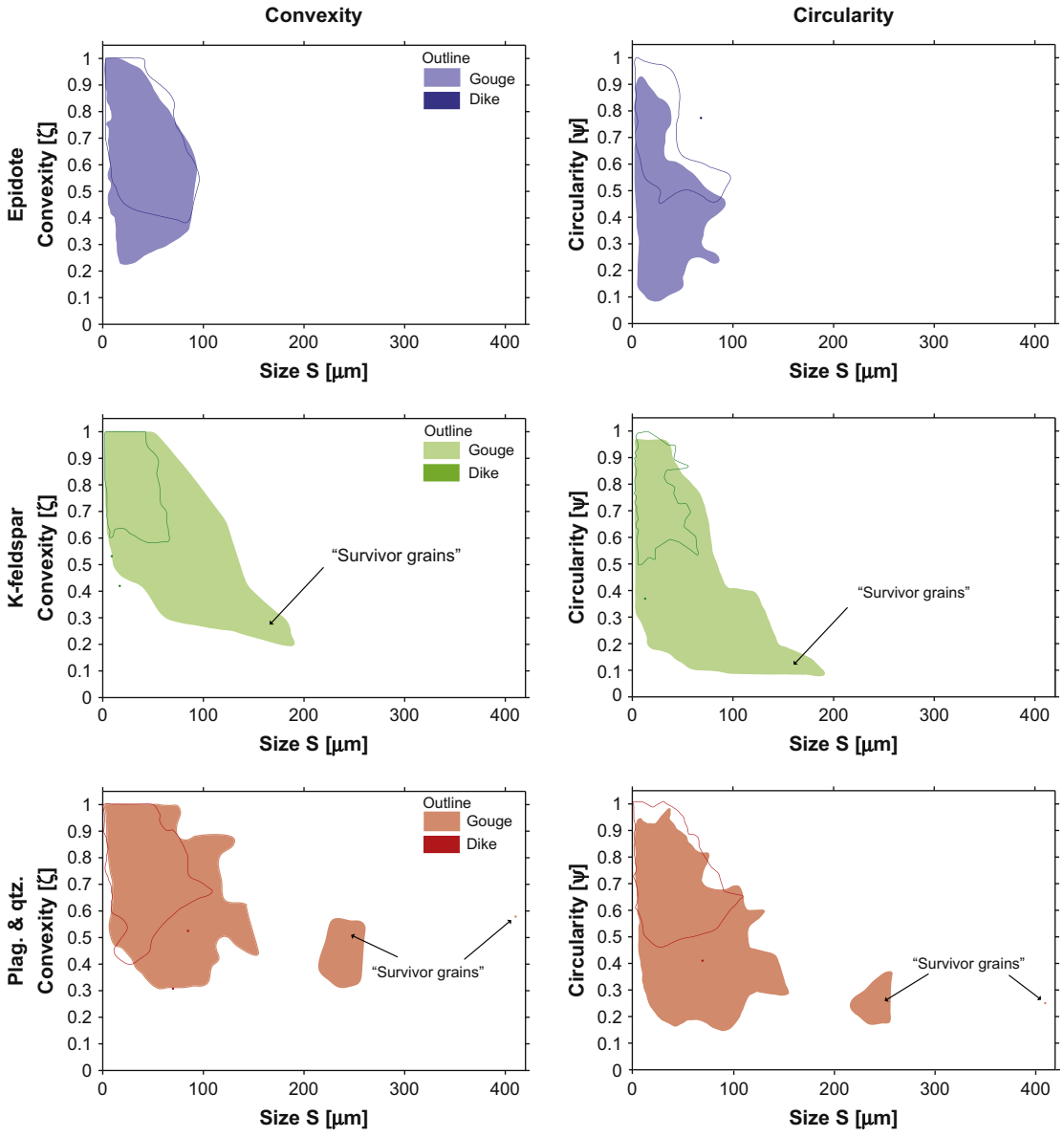

Fig. 13. Outlines of convexity, and circularity versus size (equal area diameter) for the individual mineralogical phases in the two samples based on the raw data presented in Fig. 12.

since epidote is a diagenetic mineral that has most likely formed in the dike and gouge samples late in their evolution. Importantly, in the dike sample, we find an absence of any significant fraction of the small irregular and non-spherical grains that are present in the gouge sample (Fig. 13). Instead, the dike has small spherical grains with smooth surfaces indicative of particle abrasion.

5.3. Particle size interpretations

The *D*-values for the gouge sample are generally large, with the majority of the size range fit by D_1 (2.9–3.2) and large (or small) particles best fit by D_2 (Fig. 9). Higher D_2-values are generally observed for the largest particle fraction. Laboratory experiments by Heilbronner and Keulen (2006) and Keulen et al. (2007) show similar results that they interpret as a possible switch in deformation mechanism.

The smallest fraction of epidote is fit by a smaller D_2-value of $\sim$1.8. Although such a D_2-value is comparable to that reported from extensional fractures (Marone and Scholz, 1989; Blenkinsop, 1991; Blenkinsop and Fernandes, 2000), in this context it is unlikely that this small fraction is created by a tensile fragmentation process. The low D_2-value of epidote might be due to an over-sampling of larger grains (Blenkinsop, 1991) at high magnifications or could represent the grinding limit for epidote (An and Sammis, 1994).

The D_1-values we observe in the gouge sample are generally higher than reported from theoretical fragmentation models (Allegre et al., 1982; Turcotte, 1986; Sammis et al., 1986,1987) and from lab experiments and faults in crystalline basement rocks which tend to have $D \sim 2.6$ (Biegel et al., 1989; Marone and Scholz, 1989; Sammis et al., 1986,1987; Sammis and Biegel, 1989), consistent with the constrained comminution model of Sammis et al. (1986,1987). However, importantly *D*-values may be influenced by the amount of shear displacement, number of fracturing events and confining pressure (Engelder, 1974; Sammis et al., 1986; Marone and Scholz, 1989; Blenkinsop, 1991; An and Sammis, 1994; Blenkinsop and Fernandes, 2000; Storti et al., 2003).

Our D_1-values are comparable to those reported for intensive shear localization in similar cataclastic rocks (adamellite, (gneissic) granodiorite, (gneissic) granites composed mainly of quartz, feldspars, epidote, amphibolite, mica, and chlorite by Blenkinsop (1991); An and Sammis (1994); Heilbronner and Keulen (2006); Keulen et al. (2007). The D_1-values are also comparable to other studies carried out on mono-mineralogical rocks by Marone and Scholz (1989); Blenkinsop and Fernandes (2000); Storti et al. (2003) (quartz sand, chromitite, and limestone, respectively). Recent work by Sammis and King (2007), predicts a theoretical *D*-value of 3.0 in high-strain fault gouges. Hence, we suggest in-situ shear granulation is consistent with our PSD observations.

In the dike sample, the data are fit by one single *D*-value. The *D*-values observed are generally larger than those for the gouge sample (Table 3) and are larger than those generally expected for extensional fractures (Marone and Scholz, 1989; Blenkinsop, 1991; Blenkinsop and Fernandes, 2000) or for faults in crystalline basement rocks (Biegel et al., 1989; Marone and Scholz, 1989; Sammis et al., 1986,1987; Sammis and Biegel, 1989). Similarly to the gouge sample, the *D*-values of the dike material are comparable to those reported for intensive shear localization in cataclastic rocks (Marone and Scholz, 1989; Blenkinsop, 1991; An and Sammis, 1994; Blenkinsop and Fernandes, 2000; Storti et al., 2003; Heilbronner and Keulen, 2006; Keulen et al., 2007). If the fracture filling in the dike was solely derived from tensile fracturing of the wall-rock, one would expect substantially larger grain fragments than observed in the gouge sample. Such fragments are clearly not present. In considering a purely sedimentary origin, studies of undeformed sedimentary rocks show that they do not have a fractal PSD, but are often characterized by unimodal, and bimodal PSDs (e.g. Banerjee, 1963; Church, 2003; Ethridge, 1977; Fergusson and Tye, 1999; Ferm, 1962). However, these results are not directly applicable to the dike sample in our study since they do not indicate how the transport of basin (i.e. sedimentary) material through a network of fractures may influence the final PSD.

5.4. The effects of mineralogy

It is established that *D*-values larger than 3 can be produced during intensive shear localization in both mono- and poly-mineralogical rocks. Mineralogy may be an important control on dominant deformation mechanism (e.g. fracturing versus abrasion) and the resulting size and shape distributions when the rheological properties and relative proportions of the mineral phases vary.

Blenkinsop (1991) noted that mineralogy is an important factor affecting the PSD of fault rocks. Fault rock collected from the Cajon Pass Drillhole showed systematic variation with increasing plagioclase content. The granite showed the lowest *D*-value, with *D*-values increasing in the granodioritic gneiss, and granodiorite. In the two samples presented in this study, we apparently observe the opposite result where *D*-values increase systematically. Plagioclase/quartz has the lowest value, K-feldspar has an intermediate value, while epidote has the highest value (Tables 2 and 3). This might reflect the rheological properties of the mineral phases, at least for the non-diagenetic phases. However, since plagioclase/quartz is being treated as a single phase a direct comparison may not be appropriate. As noted above, the evaluation of PSDs in relation to mineralogy is an important issue that might help us understand rock fragmentation processes better. To properly address these issues, systematic laboratory deformation experiments on a suit of mineralogically varied samples with evaluation of size and shape characteristics of the individual deformed mineral phases would be essential.

Few quantitative studies of fault rock shape characteristics exist to date, however we note that Heilbronner and Keulen (2006) and Storti et al. (2007) have conducted particle shape analyses of fault rock material. The shape analyses by Heilbronner and Keulen (2006) are not easily comparable to the shape descriptors used in this study. Storti et al. (2007) measured angularity from fault cores in limestone. Their definition of angularity ($\alpha = P^2_{\mathrm{Particle}}/A_{\mathrm{Particle}}$) where *P* and *A* are the perimeter and area, respectively) is in fact comparable to our definition of circularity $\psi = 4\pi/\alpha$ where we see that the circularity is proportional to $1/\alpha$. We suggest that the term angularity may not be optimal since this shape factor describes how close a particle's shape is to that of a circle? For example, two rectangles with different aspect ratios will qualitatively have an angular shape, but different angularity values. After clarifying these terminological distinctions, the results presented in this paper appear to be opposite to the conclusions of Storti et al. (2007). However, it is important to note the significant differences in rock type and particle size range in the respective studies. In this study we have examined fracture material in granodiorite with a particle size range of 2.21–410.22 μm, while Storti et al. (2007) have studied fracture material in limestone (mostly calcite with sub-ordered dolomite) with a particle size classes between 0.125 mm and 1.000 mm.

5.5. Field and textural observations

Both field and textural observations support in-situ granulation in the gouge sample. The relatively low apparent displacement observed in (Fig. 2) combined with the relatively high D_1-values may be reconciled by high confining pressure and/or several faulting events, involving both sinistral and dextral movement.

Repeated faulting events might be represented by the internal shear bands in the fault gouge (Fig. 4). Another possibility is that the apparent displacement observed in the field is much smaller than the actual shear displacement. We also observe fragmentation of wall-rock material (Fig. 4) consistent with in-situ granulation.

It is difficult to distinguish between wall-rock material and basin material, in the dike sample, on the basis of chemical analysis since the clasts in the Hornelen basin are lithologically identical to the rocks of the BGC (Cuthbert, 1991). However, field and textural observations can give an indication of the origin of the dike material. From the field observations it is clear that the dike is a pull-apart fracture (Fig. 3). The dikes are also connected to sub-parallel fractures with granulated material. These fractures have the same orientation (160/70, 154/72) as the fractures and faults found elsewhere in the granodiorite and in the basin (Bjørk, 2006a) and it is reasonable to assume that they are related to the basin development.

The material in the pull-apart dike has three possible origins. It is either: (i) granulated material of the wall-rock that has been transported from the connecting fractures; (ii) material derived from the basin; or (iii) a combination of both. We observe relatively large grains locally (Fig. 3). However, we also observe minor granulation in fractures connected to the dike itself (Fig. 3) and in the wall-rock of the dike sample (Fig. 6). The absence of large grains may suggest that the majority of the granulation was not in-situ, but occurred in the connecting fractures and the material was then transported into the pull-apart fractures. Since the fractures and granulation zone are thin and/or under compressive stress, transport of relatively large grains to the tensile fractures (low pressure zones) would be inhibited. At the same time, we observe flow structures in the field (Fig. 3). This is not direct evidence of basin infill, only that a pressurized fluid was present. However, the proximity to the basin margin means that infill of basin material is not unreasonable.

The field and textural observations, and particle size and shape characteristics in the dike sample show a mixed signature. Hence, we suggest the dike material has been derived from both granulation in subsidiary fractures and infill from the basin.

5.6. Coupled reaction–deformation processes

An important point, often neglected in particle analyses of fault material is the effect of mineralogy and dynamics of coupled deformation–reaction processes. In both samples, observations suggest that several minerals form during and/or after deformation in addition to epidote. Chlorite appears to be related to the faulting event since it increases in the wall-rock towards the fault gouge sample. Sericite is also found in the fracture material in both samples. These minerals are hydrous and indicate fluid transport in both samples. The role of fluids is clearly important. The mineral growth of epidote will influence both the size and shape of the grains, and treating them as non-reactant clasts that become granulated is somewhat naive.

In the gouge sample the epidote grains are zoned with iron-rich outer parts that display a complex shape, both in the wall-rock and in the gouge (Fig. 5). The shape is partly euhedral and partly irregular suggesting that the outer parts grew after cataclasis. This is strong evidence of cataclastic deformation and this implies fluid presence in the fault zone and several deformation events, otherwise there would be no reason for the epidote to grow.

The epidote in the dike sample has a comparable texture to the gouge sample, with the exception that it shows no evidence of concentric growth (Fig. 7). This does not exclude epidote growth in the connecting fractures during cataclasis, but documents that the iron-content in the fluid was comparable before and after any cataclasis. It is not unreasonable to infer that the proximity to the basin allows for substantial fluid infiltration that could buffer the iron-content in the fractures close to the basin margin. However, this buffering would be unlikely in faults and fractures, e.g. the gouge sample, ~150 m away from the basin margin. This distinction could potentially account for the differing modal percentage of epidote in the two samples. The lack of irregular epidote grains in the dike might indicate that the deformation has not involved sequential faulting events and/or that stress state of the system has favoured abrasion as the dominant deformation mechanism.

6. Conclusions

Granular material from a fault and a clastic dike in granodiorite at the NW contact zone of the Hornelen basin have been compared by a new digital image analysis tool to extract size and shape characteristics for individual mineral phases. We demonstrate the importance of incorporating both field and textural observations and the advantage of combining grain size and shape analysis with mineral phase recognition. Our results reveal quantifiable differences in the granular material. Hence a distinct origin of these materials is interpreted.

Particle size distributions measured in both samples are consistent with shear fracturing ($D \sim 3.0$–3.2). However, the shape characteristics of the two samples are distinct. The granular material from the dike shows no clear shape–size relationship. In contrast, the non-diagenetic phases in the gouge show a systematic shape–size relationship (smaller grains being circular and smoother) suggesting a shift in dominant deformation mechanism from intragranular fracturing to abrasion with decreasing grain size. This apparent change in deformation mechanism may explain the D-values larger than 3. Similarly, field observations, petrography, and the shape and texture of epidote indicate that this granular material was formed by repeated faulting events.

Field and textural observations, combined with grain size and shape characteristics indicate that the dike sample has a mixed origin. Granulation in fractures connecting to the dike indicates mechanical deformation, while flow structures, texture, grain shape, and high content of epidote, as well as the presence of other hydrous minerals in the dike itself suggest that fluids from the basin have been present. Hence, we suggest that the dike material is partly derived from granulation in connecting fractures and partly from infill of basin material due to the proximity to the basin margin.

Our results highlight the importance and added value of a combined approach incorporating phase recognition, grain size and shape analysis in granular materials. We demonstrate that particle shape measurements in addition to PSDs provide a much more effective descriptor of fault rocks. An important future step will be to adopt a standardized set of shape descriptors so different studies can be effectively and systematically compared.

The results also show that phase differentiation is extremely important. Mineralogy may control the dominant deformation mechanism and it is evident that without phase differentiation, subtle signals in PSD, and shape characteristics would not be recognized, and the bulk signal is potentially unrepresentative, particularly for the least abundant phase.

Acknowledgements

We wish to thank the reviewers, especially Andrea Billi, whose comments helped improve the manuscript. This work was financed by the Centre of Excellence for Physics of Geological Processes at the University of Oslo.

Appendix. Detailed geological map

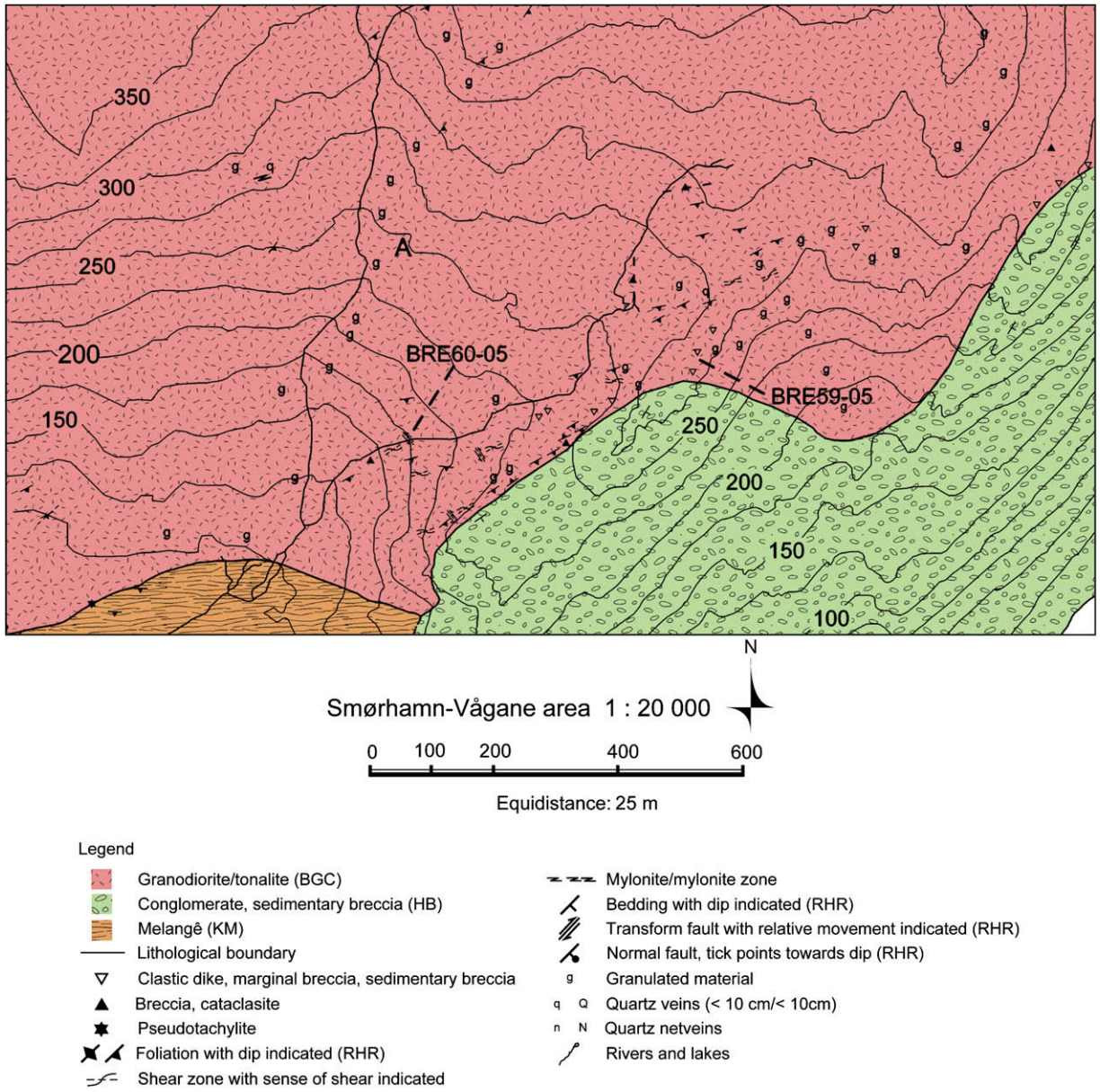

Detailed geological map of the field area (61°47′27.07″N 4°59′55.64″E).

References

Abe, S., Mair, K., 2005. Grain fracture in 3D numerical simulations of granular shear. Geophysical Research Letters 32, L05305. doi:10.1029/2004GL022123.

Allegre, C.J., Mouel, J.L., Provost, A., 1982. Scaling rules in rock fracture and possible implications for earthquake predictions. Nature 297, 47–49.

An, L.-J., Sammis, C.G., 1994. Particle size distribution of cataclastic fault material from Southern California: a 3-D study. Pure and Applied Geophysics 143, 203–227.

Andersen, T.B., 1998. Extensional tectonics in southern Norway: an overview. Tectonophysics 273, 129–153.

Antonellini, M., Aydin, A., 1994. Effect of faulting on fluid flow in porous sandstones: petrophysical properties. AAPG Bulletin 78, 355–377.

Banerjee, I., 1963. Trend of Sedimentary differentiation in Barakar sandstones of the south Karanpura coalfield, India. Journal of Sedimentary Petrology 33, 320–332.

Barrett, P.J., 1980. The shape of rock particles, a critical review. Sedimentology 27, 291–303.

Biegel, R.L., Sammis, C.G., Dieterich, J.H., 1989. The frictional properties of a simulated gouge having a fractal particle distribution. Journal of Structural Geology 11, 827–846.

Bjørk, T.E., 2006a. Quantification and Modeling of Deformation Processes: Motivated by Observations from the Contact to the Hornelen Basin, Bremangerland. Masters thesis, Physics of Geological Processes (PGP), Department of Physics, University of Oslo. http://folk.uio.no/torbjoeb/master_thesis/.

Bjørk, T.E., 2006b. Gray Scale Image Analysis. Image Analysis Program for Use with MATLAB. http://folk.uio.no/torbjoeb/image_analysis/.

Blenkinsop, T.G., 1991. Cataclasis and processes of particle size reduction. Pure and Applied Geophysics 136, 59–86.

Blenkinsop, T.G., Fernandes, T.R.C., 2000. Fractal characterization of particle size distribution in chromitites from the Great Dyke, Zimbabwe. Pure and Applied Geophysics 157, 505–521.

Blott, S.J., Pye, K., 2008. Particle shape: a review and new methods of characterization and classification. Sedimentology 55, 31–63.

Boggs, S.Jr., 1967. Measurement of roundness and sphericity parameters using an electronic particle size analyzer. Journal of Sedimentary Petrology 37, 908–913.

Brittain, H.G., 2001. Particle-size distribution part 1, representation of particle shape, size, and distribution. Pharmaceutical Technology 25, 38–45.

Bryhni, I., 1978. Flood deposits in the Hornelen basin, west Norway (Old Red Sandstone). Norwegian Journal of Geology 58, 274–300.

Chester, F.M., Evans, J.P., Biegel, R.L., 1993. Internal structure and weakening mechanisms of the San Andreas fault. Journal of Geophysical Research 98, 771–786.
Crompton, C., 2005. Particle Shape, an Important Parameter in Pharmaceutical Manufacturing. Pharmaceutical Manufacturing and Packing Sourcer. http://www.samedanltd.com/magazine/15/issue/55.
Church, M.J., 2003. Grain settling. In: Gerard, V. (Ed.), Encyclopedia of Sediments and Sedimentary Rocks. Springer, The Netherlands 336345.
Cuthbert, S.J., 1991. Evolution of the Devonian Hornelen basin, west Norway: new constraints from petrological studies of metamorphic clasts. In: Morton, A., Todd, S., Haughton, P. (Eds.), Developments in Sedimentary Provenance Studies. Geological Society Special Publications. Geological Society of London, United Kingdom, vol. 57, pp. 343–360.
Dobkins Jr., J.E., Folk, R.L., 1970. Shape development on Tahiti-Nui. Journal of Sedimentary Petrology 40, 1167–1203.
Engelder, J.T., 1974. Cataclasis and the generation of fault gouge. Geological Society of America Bulletin 85, 1515–1522.
Engvik, A.K., Bertram, A., Sťockhert, B., Austrheim, H., 2005. Magma-driven hydraulic fracturing and infiltration of fluids into the damaged host rock, an example from Dronning Maud Land, Antarctica. Journal of Structural Geology 27, 839–854.
Ethridge, F.G., 1977. Petrology, transport, and environment in isochronous Upper Devonian sandstone and siltstone units, New York. Journal of Sedimentary Petrology 47, 53–65.
Fergusson, C.L., Tye, S.C., 1999. Provenance of Early Palaeozoic sandstones, southeastern Australia, part 1: vertical changes through the Bengal fan-type deposit. Sedimentary Geology 125, 135–151.
Ferm, J.C., 1962. Petrology of some Pennsylvanian sedimentary rocks. Journal of Sedimentary Petrology 321, 104–123.
Folk, R.L., 1955. Student operator error in determination of roundness, sphericity, and grain Size. Journal of Sedimentary Petrology 25, 297–301.
Hansen, J., Skjerlie, K.P., Pedersen, R.B., 2002. Crustal melting in the lower parts of island arcs: an example from the Bremanger Granitoid Complex, west Norwegian Caledonides. Contributions to Mineralogy and Petrology 143, 316–335.
Hartz, E., Andresen, A., Andersen, T.B., 1994. Structural observations across a detachment zone in the hinterland of the Norwegian Caledonides. Tectonophysics 231 (1–3), 123–137.
Hattori, I., Yamamoto, H., 1999. Rock fragmentation and particle size in crushed zones by faulting. Journal of Geology 107, 209–222.
Heilbronner, R., Keulen, N., 2006. Grain size and shape analysis of fault rocks. Tectonophysics 427, 199–216.
Herwegh, M., de Bresser, J.H.P., ter Heege, J.H., 2005. Combining natural microstructures with composite flow laws: an improved approach for the extrapolation of lab data to nature. Journal of Structural Geology 27, 503–521.
Howard, J.L., 1992. An evaluation of shape indices as palaeoenvironmental indicators using quartzite and metavolcanic clasts in Upper Cretaceous to Palaeogene beach, river and submarine fan conglomerates. Sedimentology 39, 471–486.
Keulen, N., Heilbronner, R., Stnitz, H., Boullier, A.-M., Ito, H., 2007. Grain size distributions of fault rocks: a comparison between experimentally and naturally deformed granitoids. Journal of Structural Geology 29, 1282–1300.
Krumbein, W.C., 1941. Measurement and geological significance of shape and roundness of sedimentary particles. Journal of Sedimentary Petrology 11 (2), 64–72.
Mazzullo, J., Ritter, C., 1991. Influence of sediment source on the shapes and surface textures of glacial quartz sand grains. Geology 19, 384–388.
Marone, C.J., Scholz, C.H., 1989. Particle size distribution and microstructures within simulated fault gouge. Journal of Structural Geology 11, 799–814.
Morrow, C.A., Moore, D.E., Lockner, D.A., 2001. Permeability reduction in granite under hydrothermal conditions. Journal of Geophysical Research 106, 30.551–30.560.
Norton, M.G., 1986. Late Caledonian extension in western Norway: a response to extreme crustal thickening. Tectonics 5, 195–204.
Osmundsen, P.T., Andersen, T.B., Markussen, S., Svendby, A.K., 1998. Tectonics and sedimentation in the hanging wall of a major extensional detachment: the Devonian Kvamhesten basin, western Norway. Basin Research 10, 213–234.
Osmundsen, P.T., Andersen, T.B., 2001. The middle Devonian basins of western Norway: sedimentary response to large-scale transtensional tectonics. Tectonophysics 332, 51–60.
Powers, M.C., 1953. A new roundness scale for sedimentary particles. Journal of Sedimentary Petrology 23, 117–119.
Rønjom, S.F., 2006. Quantification and Modeling of Localized Deformation in Shear Zones and Faults: Motivated by Observations from the Contact to the Hornelen Devonian Basin, Bremangerland. Masters thesis, Physics of Geological Processes (PGP), Department of Physics, University of Oslo.
Sammis, C.G., Osborne, R.H., Anderson, J.L., Banerdt, M., White, P., 1986. Self-similar cataclasis in the formation of fault gouge. Pure and Applied Geophysics 124, 53–78.
Sammis, C., King, G., Biegel, R., 1987. The kinematics of gouge deformation. Pure and Applied Geophysics 125, 777–812.
Sammis, C.G., Biegel, R.L., 1989. Fractals, fault gouge and friction. Pure and Applied Geophysics 131, 255–271.
Sammis, C., King, G., 2007. Mechanical origin of power law scaling in fault zone rock. Geophysical Research Letters 34, L04312. doi:10.1029/2006GL028548.
Seranne, M., Seguret, M., 1987. The Devonian basins of western Norway: tectonics and kinematics of an extending crust. In: Coward, M.P., Dewey, J.F., Hancock, P.L. (Eds.), Continental Extensional Tectonics. Geological Society Special Publications No 28. Blackwell Scientific Publications, pp. 537–548.
Sibson, R.H., 1996. Structural permeability of fluid-driven fault-fracture meshes. Journal of Structural Geology 18, 1031–1042.
Smith, D.A., Cheung, K.F., 2005. Transport rate of calcareous sand in unidirectional flow. Sedimentology 52, 1009–1020.
Steel, R.J., Siedlecka, A., Roberts, D., 1985. The Old Red Sandstone basins in Norway and their deformation: a review. In: Gee, D., Sturt, B.A. (Eds.), The Caledonide Orogen: Scandinavia and Related Areas. John Wiley, New York, pp. 293–315.
Storti, F., Billi, A., Salvini, F., 2003. Particle size distributions in natural carbonate fault rocks: insights for non-self-similar cataclasis. Earth and Planetary Science Letters 206, 173–186.
Storti, F., Balsamo, F., Salvini, F., 2007. Particle shape evolution in natural carbonate granular wear material. Terra Nova 19, 344–352.
The MathWorks, 2001. Image Processing Toolbox for Use with MATLAB. User's Guide Version 3. The MathWorks, Inc., Natick, MA.
Turcotte, D.L., 1986. Fractals and fragmentation. Journal of Geophysical Research 91, 1921–1926.
Wadell, H., 1936. Volume, shape, and shape position of rock fragments in openwork gravel. Geografiska Annaler 18, 74–92.
Wintsch, R.P., Christoffersen, R., Kronenber, A.K., 1995. Fluid-rock reaction weakening of fault zones. Journal of Geophysical Research 100, 13.021–13.032.
Wilks, W.J., Cuthbert, S.J., 1994. The evolution of the Hornelen basin detachment system, western Norway: implications for the style of Late Orogemic extension in the southern Scandinavian Caledonides. Tectonophysics 238, 1–30.